The Effect of Large-Scale Convergence on the Generation and Maintenance of Deep Moist Convection

N. ANDREW CROOK AND MITCHELL W. MONCRIEFF

*The National Center for Atmospheric Research, Boulder, Colorado**

(Manuscript received 10 February 1988, in final form 15 June 1988)

ABSTRACT

The effect of large-scale convergence on the generation and maintenance of deep moist convection is examined with a numerical cloud model. The term large-scale is defined as a scale which is at least an order of magnitude greater than the convective scale. Convergence is included in the model by imposing a momentum forcing at the lowest levels of the domain. The simulations are initialized with the linear response to this forcing.

It is shown that large-scale convergence has an important effect both before and after the generation of convection. Before convection commences, the convergence lifts the atmosphere to saturation, or close to saturation, over a wide region. This means that once convection begins, the air entering the system requires little further lifting and it is demonstrated that this allows the system to maintain itself without the additional lifting that evaporative cooling produces. This is in contrast to a system which is generated in an unsaturated environment by an initial warm bubble perturbation that is often critically dependant on the lifting at low levels produced by evaporative cooling.

Large-scale convergence also has an important effect on the mature convection, with the average rainfall rate decreasing by approximately 40% when the convergence is removed. It is also shown, for systems in which the convective time scale is comparable to or larger than the time that air spends in the convergence zone, that the total vertical displacement of air in the convergence region is the important parameter in determining convective intensity.

Finally, some features of the convective structure are discussed. For the first two hours of convective activity, the low-level flow has the structure of a gravity wave in that air passes through the system and remains near the surface. The amplitude and structure of this gravity wave, which is primarily forced by evaporative cooling and low-level waterloading, is compared with the predictions of linear theory. Another feature described is the formation of convective cells some 10–15 km ahead of the main updraft and the low-level cold pool.

1. Introduction

In the past decade or so there have been a number of numerical studies that have examined the generation and structure of severe long-lasting convection (Moncrieff and Miller 1976; Thorpe et al. 1982, hereafter TMM; Dudhia et al. 1987; Nicholls 1988; Redelsperger and Lafore 1988; Rotunno et al. 1988, hereafter RKW; and several others). In general, the numerical simulations in these studies have been initialized with an atmosphere having zero vertical velocity (which will be referred to as a quiescent atmosphere) and thermodynamic and horizontal wind profiles that are typical of the conditions upstream of severe convection. This quiescent atmosphere is then perturbed by either introducing a positive temperature anomaly at low levels (the "warm bubble" method, as used by RKW) or by cooling the lowest layers (the "cold pool" method used by TMM).

Two of the studies mentioned above (TMM and RKW) have examined the changes that occur as the wind shear perpendicular to the line is altered. Both studies concluded that the optimal conditions for long-lasting convection is one in which the shear is restricted to low levels (below ~3 km). The reason that this produces the longest-lasting convection appears to be that the amount of lifting of moist air at the leading edge of the system's cold pool is maximized under these conditions. Furthermore, the climatology of midlatitude squall lines reported by Bluestein and Jain (1985) indicates that severe squall lines most often occur in environments in which the strongest shear is restricted to low levels.

The numerical studies discussed above, which begin with a quiescent environment, have emphasized the importance of the cold pool at low levels in providing the extra lifting necessary to sustain severe convection. These studies have been very important in showing how a system can maintain itself in the absence of any forcing from the larger scale. One of the major aims of the present study is to demonstrate that if a larger-

* The National Center for Atmospheric Research is sponsored by the National Science Foundation.

Corresponding author address: Dr. N. Andrew Crook, NCAR/MMM, P.O. Box 3000, Boulder, CO 80307-3000.

scale convergence exists then moist convection can be maintained without a low-level cold pool.

Only two-dimensional convection is studied in the present paper. This restriction is made partly because of computer limitations but also because it simplifies the analysis of the convective structure and intensity. The assumption of two-dimensionality means that the present work is most relevant to the generation and maintenance of squall lines. Although these lines generally exhibit a certain degree of three-dimensional structure which means that some features such as the flow between individual convective cells (which affects the propagation speed) will be missed by the two-dimensional model, it is not felt that the results pertaining to the influence of large-scale convergence on the convective system are significantly affected.

In the next section, the various methods that have previously been used to include large-scale convergence in numerical cloud models are summarized and then a new method, that uses the response to a horizontal momentum forcing, is developed. This method is tested in section 3 by applying the momentum forcing to a dry environment. In section 4 the effect of large-scale convergence on the generation and intensity of convection is examined. In section 5 the structure of the mature convective system is described.

2. Inclusion of large-scale convergence

Several different methods of including large-scale convergence have been described in the literature. For the method to approximate to the real atmosphere it should produce a convergence field that can vary in time and in space and allow a feedback between the convection and convergence field. The various methods described in the literature can be classified by the way they meet these criteria. Chang and Orville (1973) describe a scheme that can be used in a streamfunction model that produces an initial convergence field which is horizontally uniform but varies in the vertical. They found later that the initial convergence decayed with time; in Chen and Orville (1980) a scheme is described that produces a convergence field that is constant in time. No feedback is allowed between the convection and the convergence field.

Tripoli and Cotton (1980) describe a scheme that produces a convergence field that varies in both the vertical and horizontal directions. The convergence is only applied at the initial time and is not forced continually inside the domain. However, the convergence is sustained to a certain degree by the conditions applied at the lateral boundaries and, to the extent that these conditions can vary, some feedback is allowed between convection and the larger-scale convergence.

Soong and Ogura (1980) and Dudhia and Moncrieff (1987) discuss similar schemes that include only the heating and moistening effects of the large-scale convergence. Soong and Ogura (1980) in a study of GATE convection estimated a vertical profile of large-scale heating and moistening rates from observations. These rates are then applied uniformly in the horizontal and constant in time to the thermodynamic and moisture equations of the model. In Dudhia and Moncrieff (1987) only the large-scale vertical velocity is taken from observations. The effects of this lifting are then included by adding a term to the potential temperature (moisture) equation which is the product of the observed large-scale vertical velocity and the vertical derivative of potential temperature (moisture) in the model.

In a recent paper by Crook (1987), extending the work of Ross and Orlanski (1978), a large-scale convergence field was included in a two-dimensional model by initializing with a surface cold front. If wind shear exists in the plane of the simulation domain, then thermal wind balance implies that a potential temperature gradient exists perpendicular to the plane of the simulation. The front thus differentially advects potential temperature into the plane of the simulation. In order that the front stay in balance, a cross-front ageostrophic circulation must develop with convergence ahead of the front and divergence behind. In the simulations described in Crook (1987) the model was initialized with this cross-front circulation (obtained by solving a version of the Sawyer–Eliassen equation). In this way, the surface front remained quasi-steady and hence the convergence ahead of the front (in the absence of convection) also remained constant.

It is important to note that in this system the moist convection generated by the large-scale convergence can feed back onto the convergence. It was shown in Crook (1987) that the convection forces a geostrophic imbalance in the front. In returning to geostrophic balance the front oscillates in a manner such that the large-scale convergence ahead of the front changes to divergence and then convergence again (see Fig. 10, Crook 1987). This should be contrasted with the majority of the methods discussed above where the large-scale convergence field is kept constant with time. Another difference is that in Crook (1987) the large-scale lifting varies with horizontal position whereas in all of the methods discussed above, with the exception of that of Tripoli and Cotton (1980), it is constant. As will be shown herein, the horizontal variation of the large-scale vertical velocity has an important influence on the strength of the convection that is generated.

One difficulty with the method described in Crook (1987) is that the large-scale convergence can only be evaluated beforehand if the front is in geostrophic balance. If this is not the case then extra forcing terms that depend on the time rate of change of the geostrophic imbalance exist in the Sawyer–Eliassen equation (see, for example, Eq. 13, Crook 1987) and these are in general difficult to estimate a priori. An important finding of Crook (1987) was that these ageostrophic forcing terms are very important in a convec-

tive flow; in fact the vertical velocity ahead of the front could at times be an order of magnitude greater in the unbalanced front than in the initially balanced front.

For the reasons discussed above a technique for imposing large-scale convergence that does not require the constraint of geostrophic balance was sought. It is well known that internal gravity waves are an important component of the mesoscale energy spectrum and that they are undoubtedly important in generating and maintaining convection. Consequently, a technique has been developed for initializing a numerical cloud model with a mesoscale internal gravity wave. In order that the gravity wave remain constant in amplitude, a continuous forcing is necessary and in the work to be described this forcing will take the form of a momentum source/sink or equivalently, a heat source/sink. Although this forcing is somewhat artificial and must be specified a priori, the technique does give useful insight into how the mesoscale responds to an imposed forcing (be it momentum source/sink or heat source/sink). Also, as the gravity waves are of small amplitude and can be essentially described by linear theory it is straightforward to predict their amplitude for a given forcing. Finally, as discussed in section 3, the convergence fields produced by this method have some similarity to the fields that develop in a short wave propagating with the upper-level wind (for instance at 600 mb).

To commence the development of this technique, the steady linear response of an incompressible Boussinesq atmosphere to imposed horizontal and vertical momentum forcing and diabatic heating is examined. This analysis essentially follows that outlined by Lin (1987) who examined the response to diabatic heating alone. The linear equations for horizontal and vertical momentum, density and mass continuity are

$$Uu_x + U_z w + p_x/\bar{\rho} = F_u(x, z) \tag{1}$$

$$Uw_x + p_z/\bar{\rho} + g\rho'/\bar{\rho} = F_w(x, z) \tag{2}$$

$$U\rho'_x + w\bar{\rho}_z = (-\bar{\rho}/c_p\bar{T})Q(x, z) \tag{3}$$

$$u_x + w_z = 0, \tag{4}$$

where F_u is the horizontal force per unit mass (in units of Newton kg^{-1}), F_w is the vertical force per unit mass and Q is the diabatic heating rate (in units of J kg^{-1} s^{-1}). The variables u, w, p and ρ' are perturbation horizontal velocity, vertical velocity, pressure and density respectively and U is the basic horizontal wind which is a function of height only. Expressing the perturbation quantities as a sum of waveforms proportional to e^{ikx}, and making the hydrostatic assumption, Eqs. (1)–(4) can be combined into a single equation for $\hat{w}$, the complex amplitude of the vertical velocity of a mode with horizontal wavenumber k

$$\hat{w}_{zz} + (N^2/U^2 - U_{zz}/U)\hat{w} = -(1/U)\partial\hat{F}_u/\partial z + \hat{F}_w ik/U + g\hat{Q}/(c_p\bar{T}U^2), \tag{5}$$

where $\hat{F}_u$, $\hat{F}_w$ and $\hat{Q}$ are the Fourier coefficients of the horizontal force, vertical force and heating functions respectively. Note that vertical momentum forcing has a different wavenumber dependance and a 90 deg phase shift compared with horizontal momentum forcing and thermal forcing. This point will be returned to in section 5c when the effects of waterloading and evaporative cooling are compared.

The homogeneous part of Eq. (5) is often called the Taylor–Goldstein equation. Solutions to the forced problem with diabatic heating (but without momentum forcing) have been obtained by several authors (see Lin 1987, for a list of such studies). For a system with diabatic heating the density (or for a compressible atmosphere, the potential temperature) is not conserved following the motion. Since the technique will be used to study the initiation of moist convection, a desirable property is that potential temperature be conserved (cf. the warm bubble method which introduces spurious thermodynamic energy); for this reason only the atmospheric response to a horizontal momentum force will be examined. From Eq. (5) it is clear that in terms of the vertical velocity w the linear response to a horizontal momentum force F_u will be the same as that to diabatic heating Q if

$$g\hat{Q}/(c_p\bar{T}U^2) = -\frac{1}{U}\partial\hat{F}_u/\partial z. \tag{6}$$

At this juncture the technique for initiating convection is summarized. A forcing function $F_u(x, z)$ is first specified and then Fourier decomposed in the horizontal to obtain $\hat{F}_u(k, z)$. Equation (5) with $\hat{F}_w = \hat{Q} = 0$ is then solved with suitable boundary conditions (e.g., $\hat{w} = 0$ at the lower boundary and radiation conditions at the top of the domain). The variable $\hat{w}(k, z)$ is thus found which is inverse Fourier transformed to obtain $w(x, z)$. Knowing $w(x, z)$, the other perturbation quantities u, p and ρ can be found from Eqs. (2), (3) and (4). These four perturbation fields can then be used to initialize a nonlinear time-dependant cloud model.

The above technique has been used with the nonhydrostatic cloud model developed at Imperial College, London (described in Miller and Pearce 1974, and in section 3 of this work). As this model is formulated in pressure coordinates and does not make the incompressible approximation it is necessary to derive a new wave equation. From the hydrostatic version of the model in Miller and Pearce (1974), this wave equation is

$$\hat{\omega}_{pp} + [N^2/(g^2\rho_0{}^2U^2) - U_{pp}/U]\omega = -\frac{1}{U}\partial\hat{F}_u/\partial p \tag{7}$$

where $\omega = Dp/dt$. However, if the expression $\omega = -g\rho_0 w$ (ρ_0 is the base state density) and the hydrostatic equation $dp/dz = -g\rho_0$ are used then Eq. (7) transforms into Eq. (5). Thus we can solve Eq. (5) to find $\hat{w}$ and hence find $\hat{\omega}$.

The first simulations were initialized with a typical midlatitude, conditionally unstable atmosphere (described in section 4a) and a constant wind U of -15 m s^{-1}. The forcing function used was bell shaped in the horizontal and linearly varying in the vertical (going to zero 100 mb above the ground). The maximum value of F_u was 0.002 N kg^{-1}. This gave a vertical velocity field with a maximum of 8 cm s^{-1} approximately 120 mb above the lower boundary and a train of vertically propagating gravity waves above this. Upon integrating the numerical model forward in time, air parcels would move into the convergence zone and then rise to their level of condensation. Further lifting would produce convective cells. However, these cells would quickly be advected out of the convergence region by the 15 m s^{-1} mean wind and into the descending branch of the gravity wave. In this region of divergence the convective cells would rapidly decay with a timescale of about 1 h.

These early simulations may have some important implications for the strength, or lack thereof, of convection that can be generated when air flows rapidly through a convergence zone (or equivalently, when a gravity wave propagates rapidly through a relatively motionless environment). However, in the present study the main interest is in the generation of severe long-lasting convective systems; these early simulations indicated that in order to obtain such systems it is necessary for the convection to remain in the region of large-scale convergence for some time. Two ways of achieving this are

1) decrease the base state wind $U(z)$, and
2) specify a shear profile such that at some height the wind changes direction. This means that once convection has been initiated and has grown into the upper-level winds it will tend to propagate against the low-level flow.

In the present study, the second method is followed as most convective systems tend to form in an environment with some shear. It is recognized that the convective system that develops will be affected by this shear, both in the amount of low-level convergence produced by latent heating and also in the local convergence generated at the head of the outflow (as discussed by TMM and RKW). In the present study only the changes associated with a state of fixed shear are examined, in a forthcoming paper the changes that occur as the shear is altered will be discussed.

However, the second method immediately raises the problem of how to treat critical layers. At any level where the mean flow $U(z)$ vanishes, Eq. (5) becomes singular. Furthermore, the linear assumption from which Eq. (5) is derived breaks down in the vicinity of the critical layer, since any perturbation in the horizontal wind u is immediately large compared with the mean wind. However, as will be shown, even though the linear theory breaks down in the vicinity of the critical level it is still possible to obtain useful solutions in the regions away from this layer.

To proceed with the development of this technique we turn to a recent paper by Lin (1987) on the problem of thermal forcing in a shear flow. He examines the response forced in a flow with constant shear given by

$$U = \alpha z. \tag{8}$$

The critical level thus occurs at $z = 0$. The ground is defined as the level $z = -H_0$ and the forcing is only specified below a set level (defined as $z = -H_1$). A definition sketch is given in Fig. 1. Equation (5) with horizontal forcing alone becomes

$$\hat{w}_{zz} + N^2/(\alpha z)^2\hat{w} = -\frac{1}{\alpha z}\partial\hat{F}_u/\partial z. \tag{9}$$

Lin (1987) examines the response to a heating function that is constant with height below $z = -H_1$. In order to keep the analogy between thermal forcing and horizontal momentum forcing, a system will be examined which is equivalent to one in which the heating function is constant with height. From Eq. (6) this means that

$$-g\hat{Q}/(c_p\bar{T}) = U\partial\hat{F}_u/\partial z \equiv \hat{F}_{eq} \tag{10}$$

must be constant with height.

The solution to Eq. (9) in the forcing region and above is

$$\hat{w}(k, z) = Az^{0.5+i\mu} + Bz^{0.5-i\mu} - \hat{F}_{eq}(k)/N^2, \quad -H_0 \leq z \leq -H_1 \tag{11a}$$

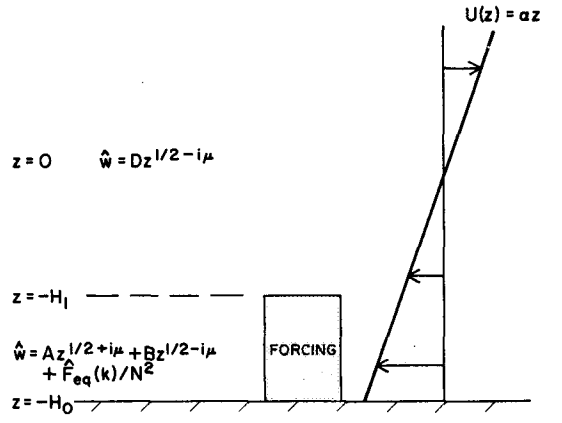

FIG. 1. Definition sketch for the response forced in a stratified shear flow. The wave solution $\hat{w}$, above and below the level of forcing $z = -H_1$, is shown.

$$\hat{w}(k, z) = Cz^{0.5+i\mu} + Dz^{0.5-i\mu}, \quad -H_1 \leq z \qquad (11b)$$

where $\mu^2 = \text{Ri} - \frac{1}{4}$, $\text{Ri} = N^2/\alpha^2$ and A, B, C and D are arbitrary constants to be determined by the boundary conditions.

Following Lin (1987) the condition for upward energy radiation is $C = 0$ (phase lines tilt upstream with height) and the lower boundary condition $\hat{w}(z = -H_0) = 0$. The system is closed by matching solutions across the top of the forcing region with the requirement that $\hat{w}$ and $\hat{w}_z$ be continuous. This leads to the following solutions for the vertical velocity components.

$$\hat{w}(k, z) = (-\hat{F}_{eq}/N^2)[0.5(1/(2i\mu) - 1) \times (-H_1)^{-0.5-i\mu}(z^{0.5+i\mu} - (-H_0)^{2i\mu}z^{0.5-i\mu} - (z/(-H_0))^{0.5-i\mu} + 1], \quad -H_0 \leq z < -H_1 \qquad (12a)$$

$$\hat{w}(k, z) = (-\hat{F}_{eq}/N^2)[0.5(1/(2i\mu) - 1) \times (-H_1)^{-0.5-i\mu}[(-H_1)^{2i\mu} - (-H_0)^{2i\mu}] + [(-H_1)^{-0.5+i\mu} - (-H_0)^{-0.5+i\mu}]]_z{}^{0.5-i\mu}, \quad -H_1 \leq z. \qquad (12b)$$

Thus for a given momentum forcing $\hat{F}_{eq}$, the linear response $\hat{w}(x, z)$ can be calculated and this can be used to initialize a nonlinear time-dependant model. Before this can be achieved it is necessary to determine the horizontal force F_u that is to be applied to the right-hand side of the horizontal momentum equation in the numerical model. From Eq. (10) above,

$$U\partial F_u/\partial z = F_{eq}$$

$$\int_z^{-H_1} dF_u = \int_z^{-H_1} F_{eq}/(\alpha z)dz$$

$$F_u(x, z) = (-F_{eq}/\alpha)\ln(-H_1/z). \qquad (13)$$

We now turn to time-dependant numerical solutions in which this forcing function F_u is applied to a shear flow.

3. Response of a dry atmosphere to momentum forcing

The horizontal form of the momentum function that will be used throughout this paper is given by

$$F_{eq} = F_{eq}^{\max}\left(\frac{b_1{}^2}{x^2 + b_1{}^2} - \frac{b_1 b_2}{x^2 + b_2{}^2}\right), \quad b_2 > b_1. \qquad (14)$$

Both terms on the right-hand side of Eq. (14) are bell-shaped functions with halfwidths of b_1 and b_2 respectively. The second term is included to ensure that no net momentum is added to the system. The horizontal variation in Eq. (14) is that used by Lin (1987) in his study of the effects of diabatic heating.

The base state velocity field $U(p)$ is plotted in Fig. 2a and the potential temperature profile given in the sounding in Fig. 2b. Note that to apply the wave solution above to a compressible system in pressure coordinates, it is necessary that $\partial U/\partial p$ be constant with height [see Eq. (7)]. The bulk Richardson number of the shear flow is 1.75. The critical layer is 282 mb or 2836 m AGL, hence $H_0 = 2836$. As can be seen above 675 mb, $U(p)$ is constant with height which means

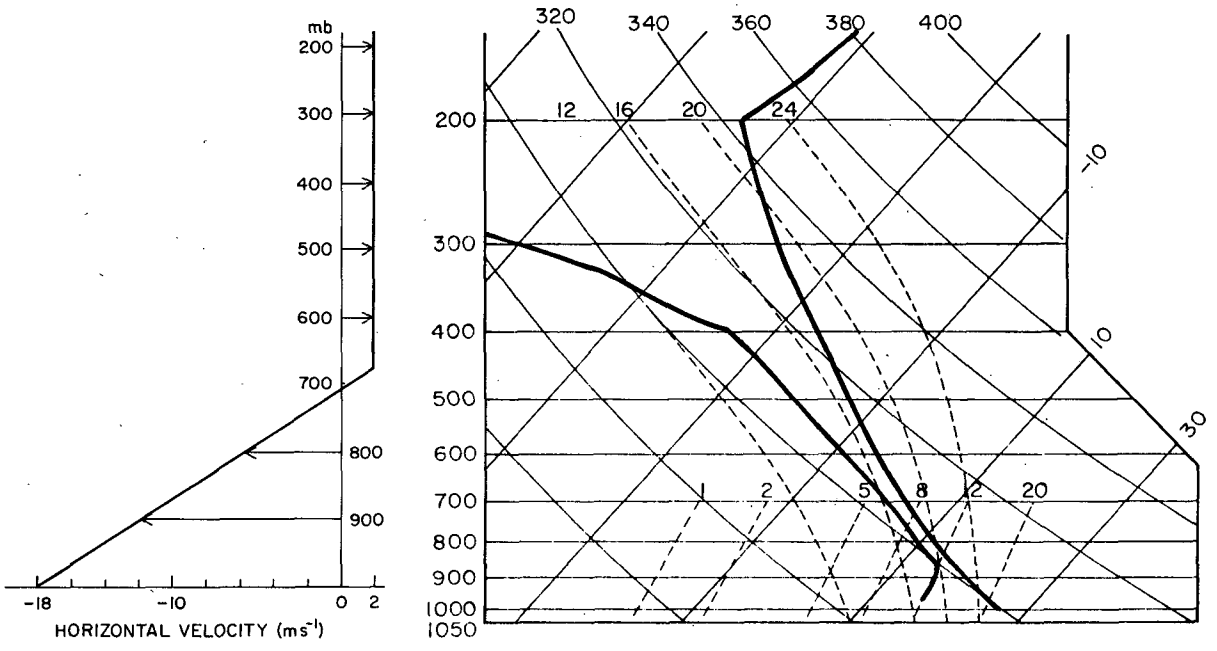

FIG. 2. (a) Base state horizontal wind used in all of the simulations. (b) Thermodynamic profile.

that the solutions given in Eq. (11) are not applicable in that region. However, as will be shown, very little energy is able to propagate through the critical layer in the steady state, hence the discrepancy introduced by assuming a constant $U(p)$ above the critical level is negligible.

The forcing function is applied over a depth of H_f = 1042 m, hence $H_1 = H_0 - 1042$ m = 1794 m. In the first simulation F_{eq}^{max} is set at 4.0×10^{-5} m s^{-3}. This gives a maximum forcing, located at the ground, of 2.75×10^{-2} m s^{-2}, which is equivalent to an acceleration of 1 m s^{-1} every 6 min. The half-width of the forcing b_1 is taken as 20 km and $b_2/b_1 = 10$. Since F_{eq}^{max} is positive the momentum forcing is equivalent to a region of negative heating [i.e., cooling, see Eq. (10)]. Again, the forcing function and the linear response (for the four fields, vertical and horizontal velocity, potential temperature and height) are included in the nonlinear model described in Miller and Pearce (1974). In all simulations the horizontal grid length is taken as 1 km and the vertical grid length as 25 mb. The model domain is 288 km long and 900 mb deep. To avoid reflections off the upper boundary a damping layer (described in Crook 1986) which has a mean damping time of 15 min is included in the upper 200 mb of the domain. The lateral boundary conditions are of the radiative type described by Miller and Thorpe (1981). Simulations with moisture use the Kessler (1969) parameterization scheme for autoconversion, accretion, rain evaporation and rainfall. Condensation and evaporation conserve energy and are assumed to act instantaneously. No supersaturation is allowed, nor can cloud exist in subsaturated conditions. Rainwater tendencies are calculated with upstream differences to help maintain positiveness; all other prognostic variables are calculated using centered differences in space. Finally, the origin $x = 0$ and hence the center of the forcing function F_{eq} are located in the middle of the domain [see Eq. (14)].

The linear solution for the given forcing is shown in Fig. 3a. As can be seen a broad region of ascending motion occurs over, and slightly upstream of, the forcing. The maximum vertical velocity is located approximately 6 km ahead of the forcing maximum. The position of this maximum depends essentially on three quantities; the shear α, and hence through Eq. (8) the horizontal wind $U(p)$, the stratification N and the depth of the forcing $H_f = H_0 - H_1$. This can be seen by first noting that the speed of the gravity waves forced in the flow is dependant on the product of the stratification and the forcing depth, NH_f. As the horizontal wind $U(p)$ is increased relative to $\sqrt{NH_f}$, the gravity waves and hence the position of the maximum vertical velocity is swept increasingly further downstream. It is thus not the shear per se that is important in this response but only the magnitude of the flow through the forcing. In other words, a similar response will be found (and has been described by Thorpe et al. 1980 and

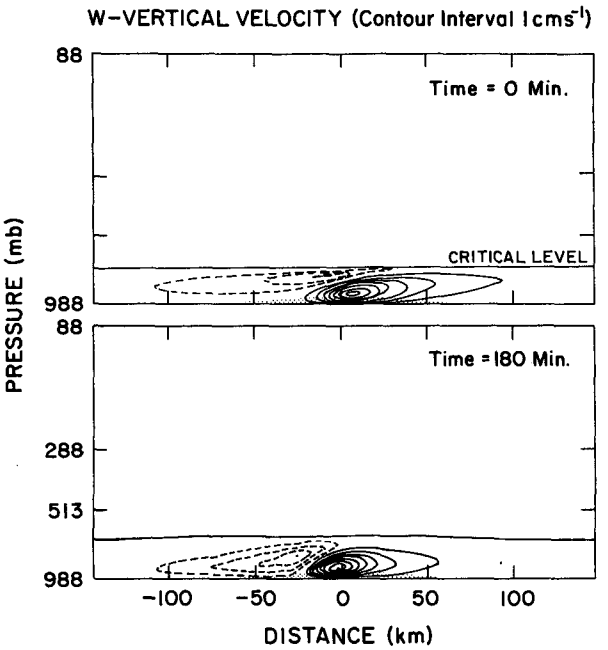

FIG. 3. (a) Linear response to an imposed momentum forcing. The shading at low levels indicates the region in which the momentum forcing is applied. The maximum value of the forcing is 2.75×10^{-2} m s^{-2}, which is equivalent to a deceleration of 1 m s^{-1} every 6 minutes. (b) The nonlinear response to the same forcing. A close examination of the critical level reveals that, in the region above the forcing, it has been lifted by approximately 300 m.

Smith and Lin 1982) for a uniform flow through a forcing region. In this system with uniform flow, the Froude number describes the ratio of the flow speed to gravity wave speed and hence determines the position of the updraft relative to the forcing.

The fact that the model is initialized with a nonzero vertical velocity field means that the horizontal shear changes with position across the domain. Far upstream the horizontal velocity is as shown in Fig. 2a with a shear of 20 m s^{-1} over the lowest 300 mb. Moving downstream the horizontal shear decreases reaching a minimum of 15 m s^{-1} over 300 mb at $x = -10$ km. This reduction in shear adds a slight complication to the analysis of moist convection generated in the domain; however, it is unavoidable in a strictly two-dimensional study which includes convergence.

As discussed previously, a response similar to that shown in Fig. 3 will be forced by a region of cooling. Indeed, as will be seen later, a similar flow pattern but with a shorter horizontal length scale occurs near the ground in a squall line in the region of evaporative cooling.

It is important to note that with the discretized numerical model it is impossible to completely resolve the linear solution in the vicinity of the critical level. The solution in Eq. (11) shows that the vertical wavelength is directly proportional to z and hence goes to

zero as the critical level is approached. Thus, within some distance of the critical level it becomes impossible to resolve the shorter vertical wavelengths. Although this may appear to be a serious defect in the discretized numerical model, as will be shown, it does not appear to substantially affect the solution below the critical layer.

The model was then integrated forward with a time step $\Delta t = 30$ sec. The first effect is that the critical layer is vertically displaced. This vertical displacement can be explained by the fact that in nonlinear theory, waves can transfer energy to the mean flow whereas in linear theory the mean state is fixed. In particular, there is a convergence of momentum at the critical level which results in an upward displacement of this level. This motion of the critical level then generates gravity waves in the layer above which subsequently propagate out of the domain as the solution relaxes to a steady state. This state (at $t = 180$ min) is shown in Fig. 3b.

The nonlinear steady-state solution is broadly similar to the linear solution. Again, there is ascent over and upstream of the forcing region. The maximum vertical velocity is almost the same (7% greater) although its position has moved downstream by 9 km. It should be noted that the nonlinear model includes vertical mixing terms that are not included in the linear model. Hence it is not surprising that some of the finer scale details in the linear solution (such as the negative velocity near the critical level above $x = 0$ and the "sharp" 0.01 m s^{-1} contour upstream of the forcing) are not included in the nonlinear solution.

The maximum vertical velocity in the domain is plotted against time in Fig. 4. The position of this maximum moves essentially in a straight line from the position shown at $t = 0$ to that shown at $t = 180$ min. As can be seen the maximum increases by about 25% in the first 40 min as the critical layer moves and then relaxes back to approximately the linear value after about 120 min.

Also plotted in Fig. 4 is the vertical velocity for a simulation in which the momentum forcing is switched off. The model with momentum forcing was run for 180 min until the nonlinear steady-state solution was obtained and then the forcing was turned off. This resulted in the gravity wave shown in Fig. 3b being swept downstream, its amplitude decreasing slowly. However, in Fig. 4 the vertical velocity at a fixed horizontal position is plotted, that being the position of maximum vertical velocity in the steady-state nonlinear solution (which occurs at $x = -3$ km). As can be seen, this velocity decreases very rapidly (with a half-time for decay of about 20 min). The reason that the vertical velocity at a fixed point is of interest, rather than the maximum, is that in some of the simulations of convection to be discussed in section 4a the momentum forcing will be switched off. In these simulations the convection is stationary relative to the domain and thus

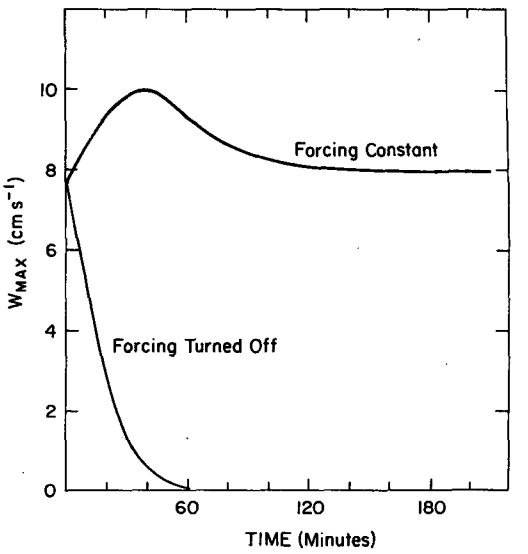

FIG. 4. Maximum vertical velocity as a function of time for two dry simulations. In the first, the momentum forcing is kept constant for the duration of the simulation. In the second, the forcing is turned off after the nonlinear steady-state solution has been reached. For this simulation the maximum velocity at a fixed horizontal position ($x = -3$ km) has been plotted and $t = 0$ has been defined as the time that the momentum forcing is turned off.

will be affected by the convergence at a fixed position and not by the region of maximum convergence which is swept downstream.

Before concluding this section we note that the convergence field shown in Fig. 3 is broadly similar to that which occurs in a short-wave trough with a horizontal length scale of approximately 150 km which is propagating with the flow at 600–650 mb. In such a short wave there is generally significant vertical motion at upper levels that is missing from the fields in Fig. 3. However, as far as moist convection is concerned, it is primarily the convergence at low levels that is important. The results presented in section 4 indicate that such a short wave moving in the shear flow indicated in Fig. 2a is very effective at maintaining moist convection since the convective cells and the short wave propagate at approximately the same speed.

4. Response of a moist atmosphere to momentum forcing

a. Initiation of convection by large-scale convergence

The convergence field shown in Fig. 3 can now be applied to a conditionally unstable atmosphere to initiate convection. The thermodynamic profile that will be used is similar to that recently studied by RKW and is shown in Fig. 2b. The profile is slightly drier at low levels (by an average of 8% below 700 mb) than that used by RKW; this drying out has been carried out for the following important reason. In many previous nu-

merical studies of convection that have used observed atmospheric soundings, the initial moisture fields have been increased in order to achieve stronger and longer-lived convection. The philosophy behind this approach has been that the observed sounding is probably not indicative of the atmosphere just prior to convection and that some lifting has most likely occurred to destabilize the atmosphere. As a method to impose this lifting is being used it is no longer necessary to commence integration with a destabilized atmosphere. Also, as discussed later in this section, if an initial perturbation such as a warm bubble is used to initiate convection in a subsaturated environment then the system that develops is sensitive, especially in the relative importance of evaporative cooling, to the initial subsaturation of the environment.

The model is initialized with the forcing and the linear response shown in Fig. 3a. The moisture profile indicated in Fig. 2b is specified uniformly in the horizontal across the domain. As the model is integrated forward, this initial moisture field is lifted in the convergence zone and the atmosphere destabilized. The forcing function F_{eq} and forcing depth have been chosen so that air in the layer between 850 and 750 mb will be lifted to just above its level of condensation. The maximum vertical displacement is 320 m and occurs for air that is originally at a height of 1.9 km; air at this level has to be lifted 260 m to its level of condensation.

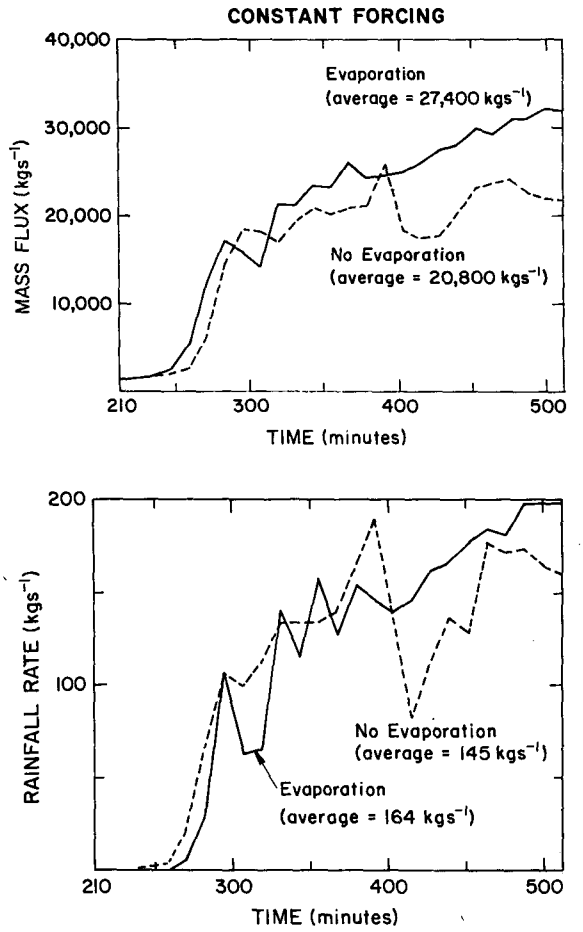

FIG. 5. (a) Maximum mass flux plotted against time for simulations 1E (with evaporation) and 1NE (with no evaporation). The data has been smoothed by applying an 8-min running average. (b) Total rainfall rate for simulations 1E and 1NE.

The maximum vertical mass flux and rainfall rate for this first experiment (simulation 1E) is shown in Fig. 5 ("E" denotes a simulation with evaporation, "NE" indicates no evaporation). The structure of this system is described in section 5a. The vertical mass flux is calculated at all vertical levels over a 60 km width that spans the maximum updraught of the system. In Fig. 5 the maximum mass flux in the vertical is plotted; generally this maximum occurs at around 500 mb. In this simulation convection begins after about 220 min (the first condensation occurs at 3 h). The simulation was terminated after 5 h of convective activity since it is the initiation and mature structure of the squall line that is of primary interest in this study and not the system's decay. (At the end of this simulation, and in fact in all of the simulations in this study except experiment 2NE, the convective system shows no sign of decay.)

As a measure of the convective intensity, averages of the maximum vertical mass flux and total surface rainfall rate are calculated. The averaging is carried out from a time 2 h after convection first breaks out (which is defined as the time when the vertical velocity first reaches 1 m s^{-1}) to the end of the simulation. For simulation 1E the average, maximum, vertical, mass flux (hereafter, average mass flux) is 27 400 kg s^{-1} and the average surface rainfall rate 164 kg s^{-1}. These values are summarized in Table 1 adjacent to the run description.

As noted in the Introduction, many previous numerical studies of squall lines that develop in quiescent environments have emphasized the importance of evaporative cooling and gust fronts in the maintenance of convection. To test the importance of evaporative cooling, an identical simulation was performed except with the term describing the evaporation of rain in subsaturated air set to zero (simulation 1NE). The maximum mass flux and rainfall rate are also plotted on Fig. 5. The average mass flux is 20 800 kg s^{-1}, which is 25% less than in the simulation with evaporative cooling. Again the system shows no sign of decay at the end of integration. As rain is allowed to fall to the ground without evaporation the *initial* rainfall rate is somewhat larger than in run 1E. However, over the full averaging period defined above, the average rate is 145 kg s^{-1}, which is 12% lower than in the simulation with evaporation.

TABLE 1. Model run description.

Run	Description	Average mass flux (kg s^{-1})	Average rainfall rate (kg s^{-1})
1E	With constant momentum forcing $F_{eq} = 4 \times 10^{-5}$ m s^{-3}, half width of 20 km	27 400	164
1NE	Same as 1E except with no evaporation	20 800	145
2E	Convection initiated with 2° hot bubble	—	—
2NE	Same as 2E except with no evaporation	—	—
3E	Momentum forcing turned off at t = 200 minutes	20 500	95
3NE	Same as 3E except with no evaporation	13 600	85
4E	Environment brought to saturation, then convergence field removed	19 800	101
4NE	Same as 4E except with no evaporation	16 500	99
4NENLW	Same as 4NE except with no waterloading below 1.5 km	15 200	94
5E	Same as 1E except half width increased to 40 km	34 300	225

It is very important to note that the convective system is not *critically* dependant on the formation of a low-level cold pool.[1] This should be contrasted with the result reported in RKW for a squall line that forms from a warm bubble perturbation in a quiescent atmosphere. They found that when the evaporative cooling term was turned off the squall line did not last beyond the lifetime of the first convective cell. To quantify this result a similar warm bubble experiment was performed in the present study. The model was initialized with a quiescent atmosphere with the structure shown in Fig. 2 and then perturbed with an identical warm bubble to that used in RKW; viz. maximum 2°C warmer than the environment, 20 km wide by 2.8 km deep. In Fig. 6 the maximum vertical velocity in the domain is plotted against time for two simulations; first with evaporative cooling (simulation 2E) and second with the evaporative cooling term turned off (simulation 2NE).

In the simulation with evaporative cooling the maximum vertical velocity oscillates strongly for the first 150 min as convective cells are generated at the cold pool and grow upward. Subsequently, the maximum vertical velocity is relatively constant as the squall system moves into a mature steady state. In the simulation with no evaporation the maximum vertical velocity is similar for the first hour of integration but after 90 min the system essentially decays.

It would be tempting to conclude from the simulations using a warm bubble that evaporative cooling is essential for the maintenance of convection. However, as has been shown when convection is initiated by a large-scale convergence zone the cooling at low levels is not essential although it does strengthen the system. The reason for this discrepancy can be summarized in the following way: *If the environmental air is lifted to its level of saturation over a wide region before the initiation of convection, then the lifting at the cold pool is no longer critical in maintaining the convective system.*

This important difference in the initiation of convection is illustrated in Fig. 7, which shows the vertical distance that air needs to be lifted before it saturates. The field is plotted at the time convection begins (which again is defined as the time when the vertical velocity first reaches 1 m s^{-1}) for the two different initiation techniques, warm bubble and large-scale convergence. As can be seen for the case with large-scale convergence

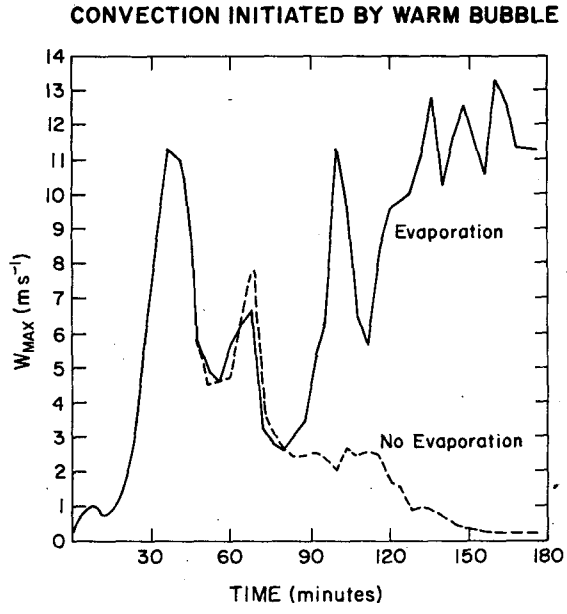

FIG. 6. Maximum vertical velocity in domain plotted against time for simulations 2E and 2NE using a warm bubble initiation process. Note that in simulations 2NE the convective system only lasts for 90 min.

[1] As well as a temperature deficit, water loading also makes a contribution to the negative buoyancy of the cold pool. However, in the simulated convection this contribution is about 30% of that due to the temperature deficit. Furthermore in section 4b (experiment 4NENLW) it will be shown that convection can be maintained without evaporative cooling or low-level waterloading, see Fig. 10.

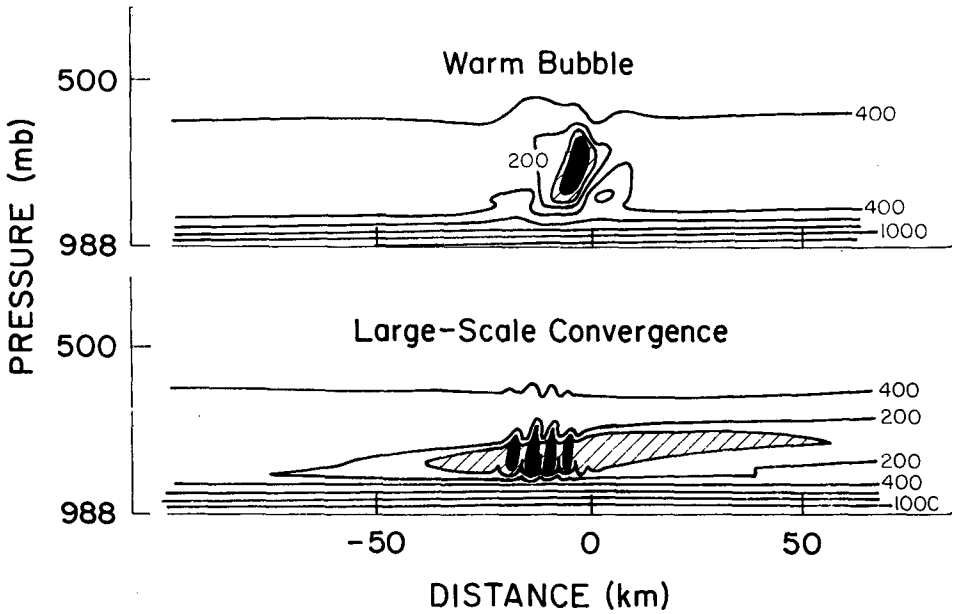

FIG. 7. The vertical distance (in meters) that air needs to be lifted to its level of condensation for the two different methods of initiation, warm bubble and large-scale convergence. The solid regions are regions of cloud, the hatched regions indicate air that has to be lifted less that 100 m.

there is a broad region (approximately 100 km wide) of air that has to be lifted less than 100 m to its level of saturation. In the warm bubble experiment this region is less than 10 km wide; most of the environment at this level (between 900 and 650 mb) has to be lifted between 200 and 400 m. Also note that just upstream of the warm bubble a dry region (approximately 10 km wide) has been produced consisting of air that has to lifted more than 400 m to saturation (a 600 m contour also occurs in this region). This dry region upstream of the initial convection does not occur in the simulations using a large-scale convergence. It is clear that, when this dry air is advected into the region where the initial condensation occurs, convection will be suppressed. It is therefore not surprising that in experiment 2 the maintenance of the squall line is dependent on the extra lifting that evaporative cooling produces.

b. *The effect of the large-scale convergence on the mature convective system*

In the previous section it has been shown that one of the important effects of large-scale convergence is to bring a wide region of the atmosphere to saturation before convection begins. However, the convergence is also important in destabilizing the environment *after* convection has been initiated. This continuing effect of large-scale convergence has been quantified by running two different experiments. In the first, the momentum forcing is set to zero when condensation first occurs. In the second experiment, the model is run with the large-scale forcing until condensation occurs, the model is then reinitialized with the destabilized environment but with the large-scale convergence and momentum forcing removed. This environment is then perturbed with a warm bubble.

In Fig. 8 the maximum mass flux and rainfall rate is plotted for simulations in which the momentum forcing is switched off at $t = 200$ min. Simulations with evaporative cooling (simulation 3E) and without cooling (3NE) have been performed. It is important to note that even though the forcing is switched off, the large-scale convergence remains for some time afterwards (as discussed previously and indicated in Fig. 4). However, this decay is quite rapid with the vertical velocity in the region of the squall line being essentially negligible 40 min after the forcing is switched off. Since the averaging period begins 140 min after the forcing is removed, it is reasonable to expect that the squall line is acting in an environment with minimal large-scale convergence.

For the squall line with evaporation the average mass flux is 20 500 kg s^{-1} and the average rainfall rate is 95 kg s^{-1}. Comparing these values with the simulation with constant large-scale convergence (1E), the removal of convergence has resulted in a 25% decrease in average mass flux and a 42% decrease in rainfall rate.

For the case with no evaporative cooling the average mass flux is 13 600 kg s^{-1} (a 33% reduction from simulation 3E) and the average rainfall rate is 85 kg s^{-1} (11% reduction). It is encouraging that these reductions

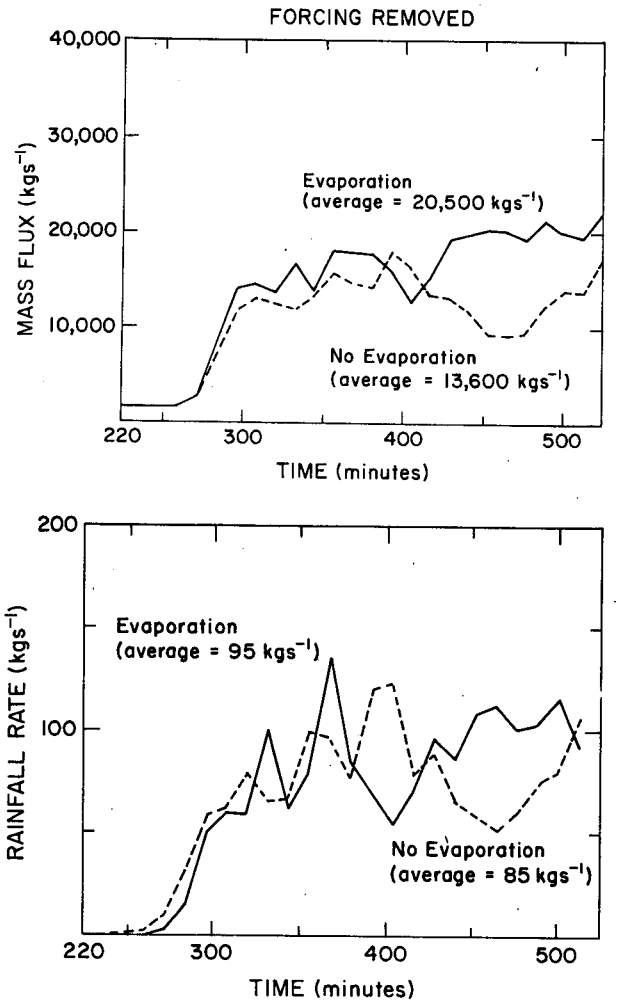

FIG. 8. Maximum mass flux and total rainfall rate for simulations 3E and 3NE in which the momentum forcing is turned off at t = 200 min.

in strength when the evaporative cooling is turned off (33% for average mass flux and 11% for rainfall rate) are comparable to the values that occur for the constant forcing simulations.

Another encouraging feature of these results can be seen by comparing the strength of the systems in the four simulations 1E, 1NE, 3E and 3NE. For this comparison the average mass flux is taken as a measure of the system intensity since the rainfall rate may not be representative in a simulation with no evaporation. In section 5c it will be argued that the responses to evaporative cooling and large-scale forcing are linear to a reasonable approximation and can thus be superimposed. Table 1 shows that when the evaporative cooling is turned off the strength of the system decreases by 25% and that a similar decrease of about 25% occurs when the large-scale convergence is turned off. In the simulation with no evaporative cooling *or* large-scale convergence the reduction in strength is 50%, which is the sum of the two separate reductions.

In the experiments discussed above, in which the forcing is switched off, the large-scale convergence persists for some time as the gravity wave decays. In an attempt to remove the convergence completely the following experiment was devised. The model was integrated forward with the large-scale convergence until saturation occurred. The atmospheric sounding at this time (Fig. 9) shows a layer of saturated air between 850 and 770 mb. Such a sounding is probably representative of the atmosphere just prior to convection in the presence of large-scale convergence; however, due to the low time and space resolution of the regular sounding network these profiles are rarely measured. One of the major conclusions of the present study is that if a cloud model is initialized with the sounding shown in Fig. 9 then the convection that develops is not critically dependant on the cooling at low levels.

The model was then reinitialized with the momentum forcing and the deviation velocity and height fields set to zero. This of course produces an unbalanced field since the large-scale convergence has produced a region of colder air in the center of the domain. When the model is integrated forward with the forcing and velocity fields set to zero, a circulation develops as this cold air descends. In the destabilized region a slight divergence is produced, whereas in the previous simulations convergence existed in this region. However, the maximum descent that occurs is only 0.02 m s^{-1}, which is significantly less than the 0.08 m s^{-1} of upward velocity that occurs in the forced flow (see Fig. 3). Furthermore, as the averaging period begins 2 h after the time when the convergence is removed, the effect of this initial imbalance is probably minimal.

The destabilized atmosphere is then perturbed with the 2° warm bubble used in experiment 2. The maximum mass flux and rainfall rates are plotted in Fig. 10 for simulations with evaporative cooling (simulation 4E) and with the evaporative cooling turned off (simulation 4NE). The average mass flux is 19 800 kg s^{-1} with evaporative cooling and 16 500 kg s^{-1} without cooling. The average rainfall rates are 101 kg s^{-1} (with evaporative cooling) and 99 kg s^{-1} (without cooling). Note that all of these values are similar to those found in experiment 3 in which just the momentum forcing is turned off.

Experiment 4NE has shown that moist convection can be maintained without the extra lifting provided by evaporative cooling or large-scale forcing if a layer of the atmosphere is first brought to saturation. However, as noted previously, waterloading also contributes to the negative buoyancy of the cold pool and thus can provide some additional lifting. To quantify this response experiment 4NE was repeated with the effects of waterloading removed below 1.5 km. The reason that experiment 4NE has been chosen for these sen-

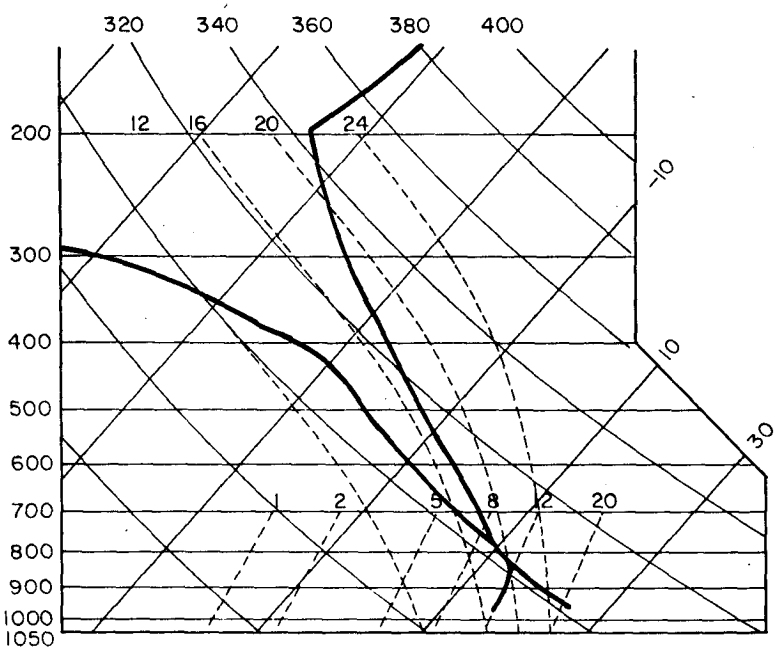

FIG. 9. Thermodynamic sounding that exists after 180 min of lifting of the sounding shown in Fig. 2b. The profiles are taken at the position $x = -10$ km. Note the layer of saturation between 750 and 850 mb.

sitivity experiments is to test if convection can be maintained solely by latent heating without any low-level lifting from waterloading, large-scale convergence or evaporative cooling.

The mass flux and rainfall rate for experiment 4NENLW (no evaporation, no low-level waterloading) are plotted in Fig. 10. The time series indicate that convection is still strong at $t = 500$ min, which shows that indeed convection can be maintained without the low-level effects listed above. The average mass flux is 15 200 kg s^{-1}, which represents an 8% reduction from experiment 4NE while the average rainfall rate is reduced by 5% to 94 kg s^{-1}.

To summarize this section, two different methods of removing the large-scale convergence once convection has been initiated have been described. Both of these methods have shown that the large-scale convergence has a significant effect *after* the generation of convection. In terms of rainfall rate, the removal of convergence has resulted in approximately a 40% reduction in strength.

c. *Further sensitivity tests with the large-scale convergence*

A number of experiments were performed with different large-scale convergence fields to examine the effect on the strength of convection. In one series of experiments, the horizontal scale and the strength of the vertical velocity field were varied in inverse proportion so as to keep the total vertical displacement in the convergence field constant. As shown by the nondimensional form of the wave solution in Lin [1987, Eqs. (19) and (20)], the total displacement depends on the product of the forcing strength F_{eq} and the width of the forcing b_1, whereas the vertical velocity depends only on the forcing strength. Thus in order to keep the total displacement fixed, the product $F_{eq}b_1$ was kept constant as the forcing width b_1 was varied. Experiments were performed with b_1 set at 10, 20 (which is simulation 1E) and 40 km. These simulations showed no significant variation in convective intensity. Experiments were also performed with the same values of b_1 except with the forcing turned off after the initiation of convection and again no significant variation in convective intensity was evident.

The simulations described above in which the vertical velocity field varies suggest that it is not the large-scale vertical velocity that is the important parameter in determining the strength of convection but the total displacement of environmental air. To further quantify this result an experiment was performed (simulation 5E) with the same maximum vertical velocity as in simulation 1 but with twice the horizontal scale, so as to double the total vertical displacement. The vertical velocity field is shown in Fig. 11. The maximum vertical displacement of air that is originally at 1.9 km is now 640 m, compared with 320 m in simulation 1. The maximum mass flux and rainfall rate are plotted in Fig. 12. The average mass flux is 34 300 kg s^{-1} which

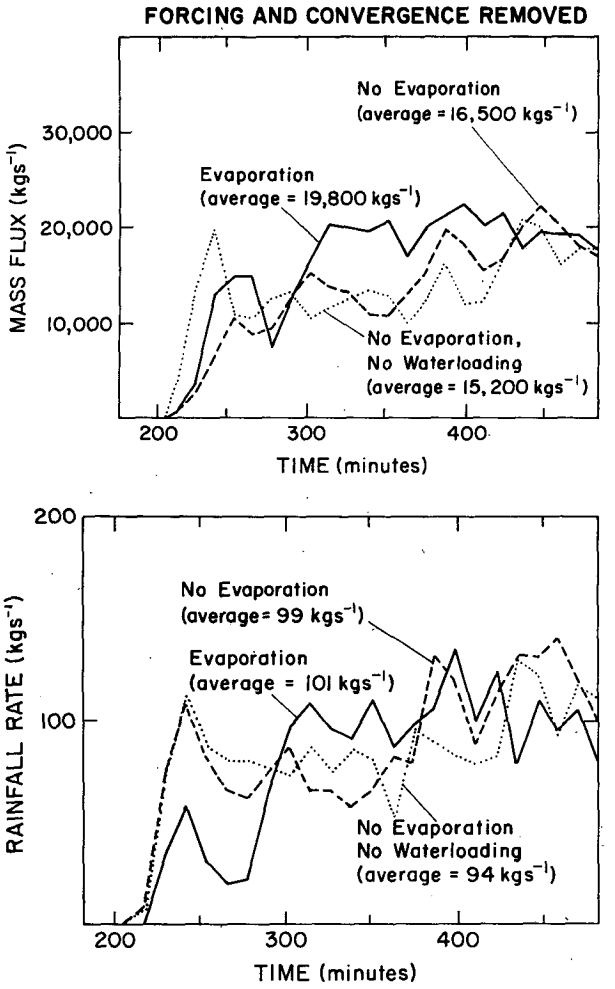

FIG. 10. Maximum mass flux and total rainfall rate for simulations 4E, 4NE and 4NENLW.

is 25% greater than in simulation 1E and the average surface rainfall rate is 225 kg s^{-1} which is 37% more.

The result that the convection is considerably more intense when the same large-scale vertical velocity is spread over a greater horizontal area is an important finding of the present work. This result should be compared with some of the methods used previously to include large-scale forcing in numerical cloud models. In the work of Soong and Ogura (1980) the large-scale vertical velocity field is effectively of infinite extent through the assumption of periodic boundary conditions. Thus, the total vertical displacement in the convergence field is infinite, a fact which would lead to obvious difficulties if the model was integrated for a long time period.

The assumption made in Soong and Ogura (1980) that the convergence zone is of infinite extent can only be justified if, for the system under study, the time scale of convection is *small* compared to the time that air spends in the convergence region. However, for the convergence zones in the present study this scale separation is not valid; a typical time that air spends in the area of convergence is about one hour. The results discussed above indicate that for systems which last as long as or longer than the time that air spends in the convergence region, one must pay particular attention to the total displacement of air in the convergence zone, rather than the vertical velocity at any one point.

5. The structure of the convective system

a. Overall flow structure

The previous sections have concentrated primarily on the initiation and maintenance of convection. In this section some aspects of the structure of the mature convective system will be examined. Attention is focused primarily on simulation 1E which contains both the large-scale forcing and evaporative cooling. The maximum mass flux and rainfall rate plotted in Fig. 5 indicates that the system is relatively steady after about 300 min. However, there are some important transient features of the circulation which will be discussed later.

For approximately the first 3 h of convective activity the squall line relative flow is of the overturning or steering-level type discussed by Moncrieff (1981) in which the air at upper levels exits ahead of the system. This is clearly shown by the streamfunction field at t = 320 min plotted in a frame of reference in which the system is stationary (Fig. 13). Although Fig. 13 depicts only the instantaneous streamfunction (and hence because of the transient features in the flow the contours cannot be viewed as trajectories) the gross pattern does not change substantially over this period of the convective activity. As can be seen, all of the outflow at upper levels is ahead of the system, conse-

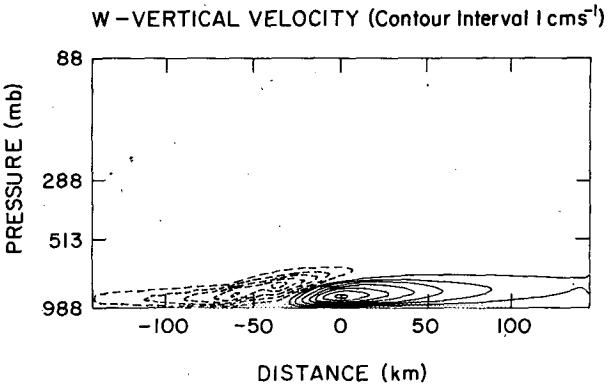

FIG. 11. Large-scale vertical velocity field used to initiate convection in simulation 5E. The field shown is the nonlinear solution, i.e., the transient features discussed in section 3 have propagated out of the domain. The momentum forcing, which is indicated by the light shading, has a half-width b_1 = 40 km.

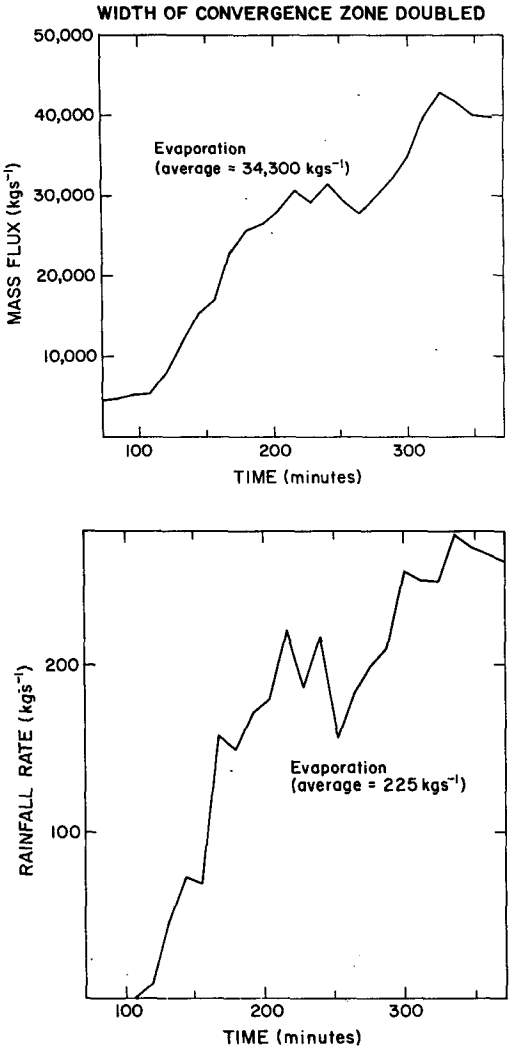

FIG. 12. Maximum mass flux and total rainfall rate for simulation 5E in which the displacement in the large-scale convergence field is doubled compared to simulation 1E. The average rainfall rate is approximately 40% larger than in simulation 1E.

quently the anvil extends forward from the convective region.

Later in the simulation some of the outflow air begins to exit from the rear of the system. This is evident in the streamfunction field (Fig. 14) and cloud water field at $t = 540$ min, which shows the development of a rear anvil. This branch of the flow is of the "jump" type described by Moncrieff (1981).

b. *The development of a density current*

Since the maintenance of convection by low-level forcing is one of the main themes of this study, it is worthwhile to examine the forcing that is produced by low-level evaporative cooling. In the early stages of convective activity the air at the surface flows *through* the region of evaporative cooling and remains at the surface.[2] The cold air that forms near the ground has often been described in the literature as a density current; however, at this stage of the motion this description is inaccurate since there is no point where the air is brought to rest relative to the system. In a density current, for example those studied in the laboratory by Simpson and Britter (1980), a stagnation point exists at the nose of the current; behind the nose the relative surface flow in the density current is *toward* the stagnation point.

However, in the simulations at this early stage of motion, the surface air is decelerated as it passes through the rain curtain which is a result of the increase in hydrostatic pressure associated with the cold air at the surface. This deceleration produces, by continuity of mass, ascent in the region of the rain shaft. This response will be termed *a gravity wave without stagnation.*

A stagnation point eventually forms at $t = 300$ min, which is after about 100 min of convective activity. With time, this stagnation point splits into two points that slowly move apart. Between these two stagnation points and beneath the streamline joining the points is a region of recirculating fluid or rotor circulation. Again, this feature can not be described as a density current since the surface air returns to the surface behind the system. The low-level flow is more accurately described as a *gravity wave with stagnation.*

The amplitude of the gravity wave subsequently builds, and the horizontal scale of the rotor grows until a time is reached when the surface air upstream of the system does not return to the surface behind the system. A trajectory analysis was performed to determine the exact time of this transition. Air parcels originating at the surface and at the leading edge of the cold pool were tracked forward with time. The first time that such an air parcel failed to return to the surface behind the system was at $t = 340$ min. In the authors' opinion, it is only after this time that the cold air at the surface can be properly described as a density current.

The three different regimes of low level flow (gravity wave without stagnation, gravity wave with stagnation and density current) are shown schematically in Fig. 15a–c. These regimes have been discussed previously by Dudhia et al. (1987) and Lafore and Moncrieff (1989). In one of the simulations presented in Dudhia et al. (1987) of a West African squall line with strong low-level shear and weak reverse shear aloft, the flow

[2] It is important to note that although the low-level flow at this stage passes through potential temperature surfaces and passes from one side of the rain curtain to the other, there is no relative horizontal motion between rain and air (by model assumption). It is only the relative vertical motion between rain and air that allows the low-level air to pass through the rain curtain.

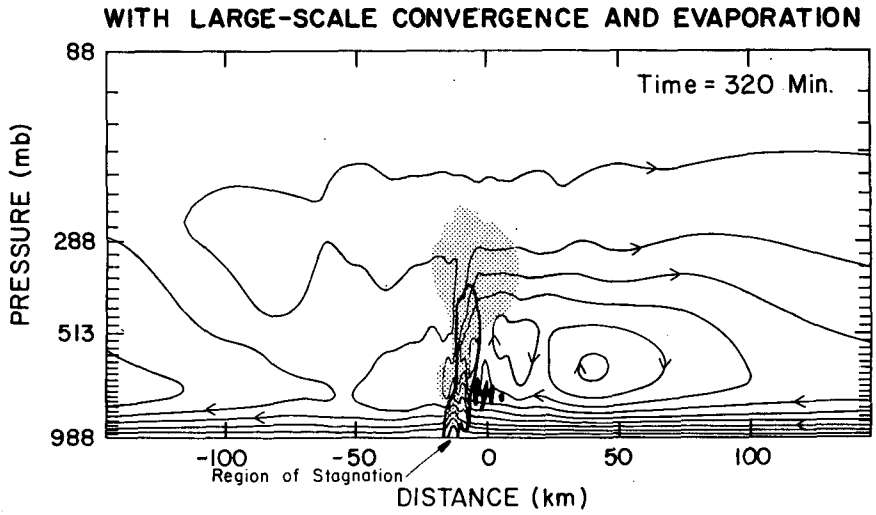

FIG. 13. The instantaneous streamfunction, in a frame of reference in which the squall line is at rest, for simulation 1E at t = 320 min (contour interval 4×10^4 kg s^{-3}). The thick solid line is the 1 g kg^{-1} contour of rainwater. The shaded region indicates cloud water concentrations greater than 0.1 g kg^{-1}. The cells forming upstream of the main updraft have been indicated by heavier shading.

at low levels remained of the gravity wave type for the entire integration. No stagnation point in the low-level flow formed over the entire simulation, which was integrated out to 14 h.

Observations of a squall line with no stagnation point in the low-level flow have also been presented recently by Fankhauser (personal communication). The squall line was observed on 20 June 1981 in the CCOPE experiment in southeastern Montana. As the squall line propagated through the observational region the surface network indicated that the low-level flow passed through the leading edge of the cold pool. Furthermore, a radar analysis approximately 1¼ h after the generation of the line also showed no stagnation point in the low-level flow.

Radar analysis of the Kansas PreSTORM squall line at 0605 UTC 27 May 1985 indicates that the low-level flow at this time had the structure of a gravity wave without stagnation. This particular squall line is currently being analyzed and simulated numerically; the results of this study will be reported in a future paper with R. Carbone and J. Conway. Finally, in a recent study by Tripoli (1987) of orogenic convective systems it was found that both the observed system and the numerically modeled system exhibited flow through the cold pool.

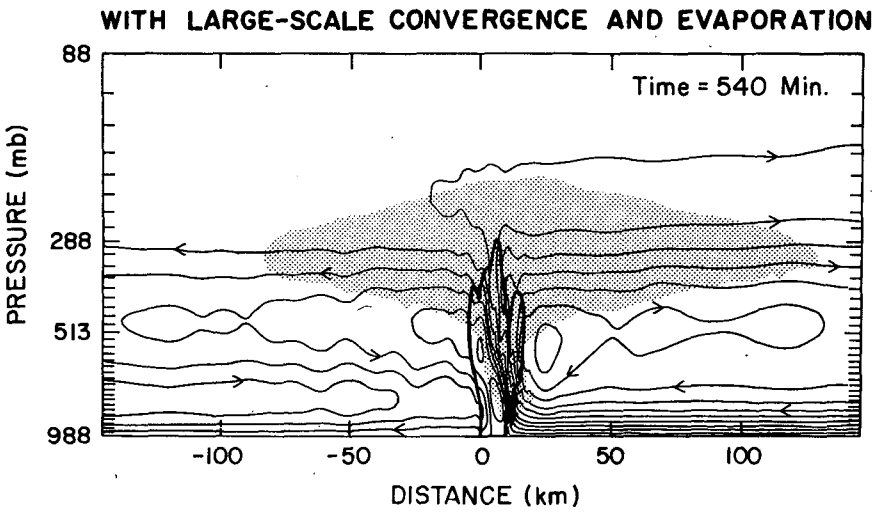

FIG. 14. As in Fig. 13 except at t = 540 min.

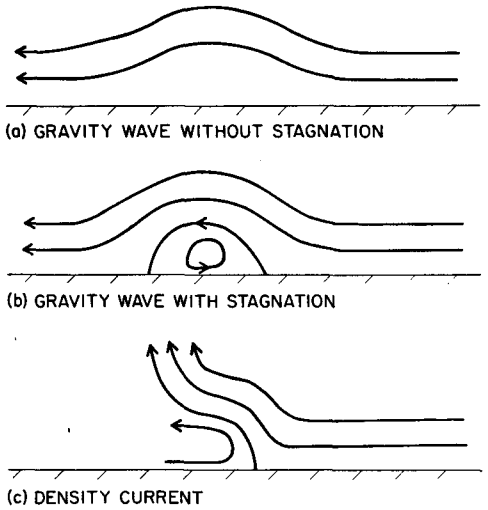

FIG. 15. Schematic representation of the three regimes of low-level flow. In (c) the air ahead of the system is shown being lifted in the system's updraft, however at early stages of this regime some of this air is circulated into the cold pool.

c. *Comparison with linear theory*

The rain water and streamfunction field for experiment 1E at t = 320 min (Fig. 13) indicates that the low-level gravity wave forms in the rain shaft with ascent in the upstream half of the shaft and descent behind. This suggests that the response is forced by evaporative cooling and waterloading. This hypothesis is further supported by the experiments in which these effects are turned off. In the experiments with no evaporative cooling (1NE, 3NE and 4NE) the amplitude of the low-level response is reduced to about 30% of that in the equivalent experiment with evaporation. In the experiment with no evaporative cooling *or* low-level waterloading (4NENLW) there is very little response forced in the flow below cloud base. The streamfunction and cloud field at t = 320 min for experiment 4NENLW is shown in Fig. 16, and as can be seen, the air below about 1.5 km passes through the convective system unimpeded.

In this section the amplitude of the low-level gravity wave will be compared with the linear theory developed in section 2 for the low-level response forced in a shear flow. Comparisons will be performed on experiments 4E and 4NE, since they contain no large-scale forcing. These experiments still retain some forcing of the low-level flow by waterloading which could be analyzed by examining the response to a vertical momentum forcing. However, as previously discussed, a vertical force has a different wavenumber dependance and a 90 deg phase shift in response compared with evaporative cooling and horizontal momentum forcing. For this reason, only the response to evaporative cooling will be examined, which will be done by examining the *reduction* in wave amplitude between experiments 4E and 4NE. This approach can be justified if the forced responses are linear, for then the effects of waterloading and evaporative cooling are simply additive.

To proceed with this analysis two assumptions must be made. First, that the only forcing of the flow below cloud base in experiment 4E is by evaporative cooling and waterloading and the only forcing in experiment 4NE is by waterloading. In both simulations latent heating exists above cloud base; however, the streamfunction field for experiment 4NENLW shows that this produces only a small response in the flow below cloud base. The second assumption is that the maximum

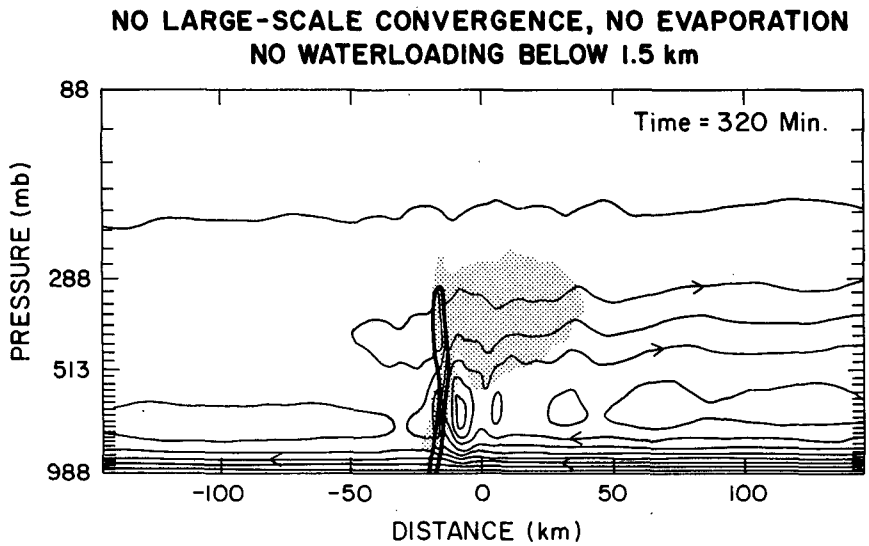

FIG. 16. As in Fig. 13 except for simulation 4NENLW.

vertical velocity in the forced response occurs at the top of the forcing. Figure 3 shows that this is reasonable assumption.

In experiment 4E the maximum vertical velocity just below cloud base (and thus at the top of forcing due to evaporative cooling) averaged over a period from t = 310 min to t = 330 min is 4.5 m s^{-1}. In experiment 4NE the average velocity at the same level and over the same time period is reduced to 1.4 m s^{-1}. A further assumption must now be made to compare with linear theory which is that the cooling is bell-shaped in the horizontal and constant below cloud base; to a first order this is a reasonable approximation. In experiment 4E the maximum cooling rate in the rainshaft averaged over 310 to 330 min is -0.02°C s^{-1} or $Q_{\text{evap}} = c_p \times -0.02 = -20$ J kg^{-1} s^{-1}. From Eq. (10) this is equivalent to a horizontal forcing function $F_{eq} = -gQ_{\text{evap}}/(c_p\bar{T}) = 6.5 \times 10^{-4}$ m s^{-3}. The large-scale convergence field shown in Fig. 3 was produced by a horizontal force, which had $F_{eq} = 4.0 \times 10^{-5}$ m s^{-3}; thus the magnitude of the forcing due to evaporative cooling is approximately 16 times that of the large-scale forcing. The evaporative cooling also occurs over a slightly greater depth ($\sim$1.5 km) than that of the momentum forcing ($\sim$1.0 km).

Substituting a value of $F_{eq} = 6.5 \times 10^{-4}$ m s^{-3} and $H_0 - H_1 = 1500$ m into Eq. (12) gives a maximum vertical velocity of 2.0 m s^{-1}. As noted above, in experiment 4 the maximum vertical velocity below cloud base falls from 4.5 to 1.4 m s^{-1} when evaporative cooling is turned off. This reduction of 3.1 m s^{-1} is greater than that predicted by linear theory, but certainly of the right magnitude. It should also be noted that even if all of the assumptions listed above were met, then an exact agreement should not be expected because of the nonlinearity of moist convection. In other words, when the evaporative cooling is turned off, the lifting of low-level air is reduced, which reduces the amount of condensation that in turn reduces the rainfall rate which (finally) reduces the lifting produced by water-loading.

It has been shown that the maximum vertical velocity forced by evaporative cooling is 2 m s^{-1}, at least an order of magnitude greater than the large-scale vertical velocity. However, as discussed in section 4c, it is the total vertical displacement in the convergence region that is the important parameter in determining the strength of convection and not the vertical velocity at any fixed point. The total displacement is directly related to the streamfunction and, as noted above, for a given shear flow this depends on the product of the forcing strength and the forcing width.

In Fig. 17 the total vertical displacement on the large scale is compared with that forced by evaporative cooling in run 1E. On the large-scale $(Qb_1)_{\text{large-scale}} = 1.2$ J kg^{-1} s^{-1} $\times$ 20 km = 2.4×10^4 m^3 s^{-3}. For the evaporative cooling, b_{evap} has been estimated by measuring

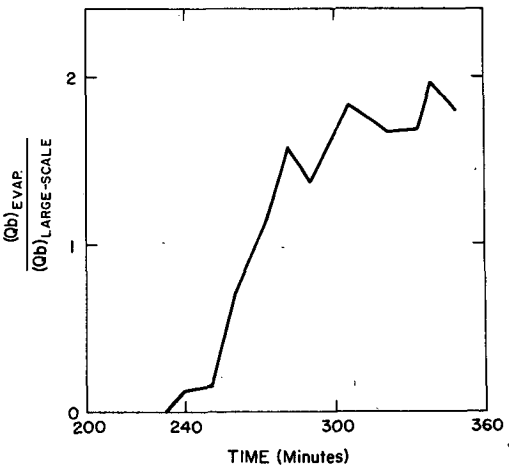

FIG. 17. Comparison of the product of the forcing strength Q and half-width b for the two forcings, evaporative cooling and large-scale momentum forcing. In linear theory the total vertical displacement in the convergence field is proportional to the product Qb.

the distance from the maximum to the point where the cooling rate is half of the maximum. This ratio has only been plotted up to 340 min, which is approximately the time when the squall line changes from a gravity wave to a density current regime. As can be seen, over the interval 280 to 340 min the total displacement caused by evaporative cooling is about 1.5–2 times as large as that occurring on the large scale. It is interesting to compare these values with the reduction of convective strength that occur when evaporative cooling/large-scale convergence are turned off. As Table 1 shows, the reduction in average mass flux when evaporative cooling is turned off is the same as the reduction that occurs when the large-scale convergence is removed. Although these averages are calculated over a longer time period and include a time when the low-level flow is not of gravity wave type it is encouraging that the ratio of these reductions (1.0) is of the same order as the ratio of displacements caused by evaporative cooling to that caused by large-scale convergence (1.5 $\sim$ 2.0).

d. Cell development ahead of the main updraft

Figure 13 shows some weak cells forming ahead of the main updraft. With time these cells grow in amplitude as they propagate backwards into the main line. This upstream development of convection is a commonly observed feature of squall lines (Fankhauser, personal communication; Srivastava et al. 1986). This development is often very intense whereas in the present simulations only weak convection occurs ahead of the main line. However, as will be argued below, the upstream development depends on a sensitive balance between the lifting induced by latent heating and the compensating subsidence. In other words, stronger up-

stream development may occur for small changes in the initial conditions, such as the initial moisture field or velocity profile.

It should be first noted that the upstream development is not caused by cooling at low levels since the development exists in the simulations with no evaporative cooling. Furthermore, the upstream development is not caused by the *continuing* effects of large-scale lifting since it also occurs in the simulations in which the convergence is turned off. The reason that convection develops some distance upwind of the main updraft is due to the fact that the environmental air has been lifted close to saturation over a wide region before convection breaks out. Hence once convection begins, the air entering the system is very close to saturation and thus any small perturbation ahead of the main line can cause cells to develop. The instantaneous streamfunction in Fig. 13 shows that the small perturbation that triggers cells are transient features associated with the compensating subsidence.

When convection first breaks out, compensating subsidence occurs close to the initial cell and then propagates away in the form of a deep gravity wave (which has a vertical half-wavelength comparable to the depth of the troposphere). As can be seen from Fig. 13 after the subsidence branch of the wave has propagated away some ascent occurs close to the system (Fig. 13 in fact shows two region of subsidence and two regions of ascent). It is when ascent exists close to the squall line system that upstream development of convection is most likely to occur. Ascent occurs close to the system when the upward mass flux in the squall line is relatively low (conversely strong descent occurs outside of the squall line when the convective flux is high). *Hence the upstream development is most likely to occur when the convective flux is weak.* Unfortunately, the method of calculating the vertical mass flux is not capable of showing any rapid changes in convective flux since the flux is calculated over a 60 km domain and hence includes the region of ascent just ahead of the squall line where the cells are developing. However, an examination of the time series of maximum vertical velocity reveals that at $t = 320$ min the maximum velocity is low (10 m s^{-1}) whereas 20 min later the maximum reaches 15 m s^{-1}.

6. Conclusions

The generation and structure of deep moist convection in a large-scale convergence field has been examined with a two-dimensional version of the Imperial College cloud model. The major results of this work are listed below.

1) The linear response of a dry stratified shear flow to a momentum forcing has been obtained. When a nonlinear time dependant model is initialized with the linear solution some unsteadiness occurs as energy propagates through the level where the base state velocity is zero. However, as Figs. 3 and 4 show, once these transient features have propagated away, the structure of the flow is very similar to the linear solution.

2) Convection has been initiated by applying a momentum forcing with a half-width of 20 km to a conditionally unstable atmosphere. It has been shown that the maintenance of convection is not critically dependant on evaporative cooling. This is in contrast to the convection that develops from a "warm bubble" perturbation in a subsaturated environment which is often critically dependant on evaporative cooling at low levels. The reason for this difference is that when a large-scale convergence is used to initiate convection, the air is first lifted to saturation over a wide area whereas a warm bubble produces saturation only in a small localized area (see Fig. 7).

3) The effects of large-scale convergence on mature convection have been examined by running two types of experiments in which the convergence is removed after the squall line is generated. Both experiments indicate that the continuing effects of convergence are significant with the rainfall rate decreasing by approximately 40% when the convergence is removed.

4) The convective intensity is not only sensitive to the large-scale vertical velocity but also the horizontal distance over which that vertical velocity occurs. It has been shown that it is the total vertical displacement in the convergence zone which is the important parameter in determining the strength of convection. This fact should be taken into account when studying systems in which the time scale of convection is comparable to or larger than the time that air spends in the convergence zone.

5) For the first 100 min of convective activity the surface air passes through the rain curtain and remains at the surface. The low-level flow structure at this stage has been termed "gravity wave without stagnation." Later in the simulation a stagnation point forms so that the surface air leaves the ground but returns some distance behind the convective system. This behavior has been termed "gravity wave with stagnation." Still later in the simulation the surface air leaves the ground and does not return but is lifted in the updraft and exits at some, nonzero, height above the ground; the term "density current" is the best description of the low-level flow structure at this time. The three different flow regimes are illustrated in Fig. 15.

6) The linear theory for the response to a thermal forcing (section 2) has been applied to the low-level flow when it exhibits gravity wave structure. For the evaporative cooling rates obtained in the numerical simulations, linear theory predicts a maximum vertical velocity of approximately 2 m s^{-1}. However, it is difficult to compare this result with the response obtained

in the numerical simulations because of the nonlinearity of moist convection; i.e., the increased lifting induced by evaporative cooling increases the rainfall rate which in turn forces a greater response in the low-level flow.

7) At certain times in the motion of the squall line, convective cells develop some distance (~10 km) ahead of the main updraft and the low-level cold pool. The development of these cells is directly linked to the fact that the air entering the convective system is very close to saturation. Therefore any small perturbation ahead of the main line can produce condensation. In the present simulations these small perturbations take the form of transient features in the compensating subsidence.

Acknowledgments. Discussions with Y.-L. Lin in the early stages of this work are gratefully acknowledged, as are the comments of R. Rotunno, who suggested experiment 4NENLW.

REFERENCES

Bluestein, H. B., and M. H. Jain, 1985: Formation of mesoscale lines of precipitation: Severe squall lines in Oklahoma during the spring. *J. Atmos. Sci.*, **42**, 1711–1732.

Chang, S. W., and H. D. Orville, 1973: Large-scale convergence in a numerical cloud model. *J. Atmos. Sci.*, **30**, 947–953.

Chen, C. H., and H. D. Orville, 1980: Effects of mesoscale convergence on cloud convection. *J. Appl. Meteor.*, **19**, 256–274.

Crook, N. A., 1986: The effect of ambient stratification and moisture on the motion of atmospheric undular bores. *J. Atmos. Sci.*, **43**, 171–181.

——, 1987: Moist convection at a surface cold front. *J. Atmos. Sci.*, **44**, 3469–3494.

Dudhia, J., and M. W. Moncrieff, 1987: A numerical simulation of quasi-stationary tropical convective bands. *Quart. J. Roy. Meteor. Soc.*, **113**, 929–967.

——, —— and D. W. K. So, 1987: Two dimensional dynamics of West African squall lines. *Quart. J. Roy. Meteor. Soc.*, **113**, 121–146.

Kessler, E., 1969: On the distribution and continuity of water substance in atmospheric circulation. *Meteor. Monogr.*, **10**(32), Amer. Meteor. Soc.

Lafore, J.-P., and M. W. Moncrieff, 1989: A numerical investigation of the scale interaction between a tropical squall line and its environment. *J. Atmos. Sci.*, **46**, in press.

Lin, Y.-L., 1987: Two-dimensional response of a stably stratified shear flow to diabatic heating. *J. Atmos. Sci.*, **44**, 1375–1393.

Miller, M. J., and R. P. Pearce, 1974: A three-dimensional primitive equation model of cumulonimbus convection. *Quart. J. Roy. Meteor. Soc.*, **100**, 133–154.

——, and A. J. Thorpe, 1981: Radiation conditions for the lateral boundaries of limited area numerical models. *Quart. J. Roy. Meteor. Soc.*, **107**, 615–628.

Moncrieff, M. W., 1978: The dynamical structure of two-dimensional steady convection in constant vertical shear. *Quart. J. Roy. Meteor. Soc.*, **104**, 543–567.

——, 1981: A theory of organized steady convection and its transport properties. *Quart. J. Roy. Meteor. Soc.*, **107**, 29–50.

——, and J. S. A. Green, 1972: The propagation and transfer properties of two-dimensional steady convection in constant vertical shear. *Quart. J. Roy. Meteor. Soc.*, **98**, 336–353.

——, and M. J. Miller, 1976: The dynamics and simulation of tropical cumulonimbus and squall lines. *Quart. J. Roy. Meteor. Soc.*, **102**, 373–394.

Nicholls, M. E., 1988: A comparison of the results of a two-dimensional simulation of a tropical squall line with observations. *Mon. Wea. Rev.*, **115**, 3055–3077.

Redelsperger, J.-L., and J.-P. Lafore, 1988: A three-dimensional simulation of a tropical squall line: convective organization and thermodynamic vertical transport. *J. Atmos. Sci.*, **116**, 1334–1356.

Ross, B. B., and I. Orlanski, 1978: The circulation associated with a cold front. Part II: Moist case. *J. Atmos. Sci.*, **35**, 445–465.

Rotunno, R., J. B. Klemp and M. L. Weisman, 1988: A theory for severe long-lasting squall lines. *J. Atmos. Sci.*, **45**, 463–485.

Simpson, J. E., and R. E. Britter, 1980: A laboratory model of an atmospheric mesofront. *Quart. J. Roy. Meteor. Soc.*, **106**, 485–500.

Soong, S. T., and Y. Ogura, 1980: Response of trade wind cumuli to large scale processes. *J. Atmos. Sci.*, **37**, 2035–2050.

Smith, R. B., and Y.-L. Lin, 1982: The addition of heat to a stratified air stream with application to the dynamics orographic rain. *Quart. J. Roy. Meteor. Soc.*, **108**, 353–378.

Thorpe, A. J., M. J. Miller and M. W. Moncrieff, 1980: Dynamical models of two-dimensional downdraughts. *Quart. J. Roy. Meteor. Soc.*, **106**, 463–484.

Srivastava, R. C., T. W. Matejka and T. J. Lorello, 1986: Doppler radar study of the trailing anvil region associated with a squall line. *J. Atmos. Sci.*, **43**, 356–377.

——, —— and ——, 1982: Two-dimensional convection in non-constant shear: A model of mid-latitude squall lines. *Quart. J. Roy. Meteor. Soc.*, **108**, 739–762.

Tripoli, G. J., 1987: Scale interaction within a developing mesoscale convective system. *Proc. of Third Conf. of Mesoscale Processes*, Amer. Meteor. Soc., 131–132.

——, and W. R. Cotton, 1980: A numerical investigation of several factors contributing to the observed variable intensity of deep convection over south Florida. *J. Appl. Meteor.*, **19**, 1037–1063.